NESTOR, a neutrino astroparticle physics laboratory for the Mediterranean

S. Loucatos*
SPP DAPNIA
CE Saclay 91191 Gif sur Yvette - France
Representing the NESTOR Collaboration †

ABSTRACT

NESTOR is a project aiming to build a deep sea neutrino telescope eventually reaching the sensitive size of one cubic kilometer. The first step of this modular detector is a tower of 20000 km^2 sensitive area [1, 2].

1 Introduction

The cosmic ray spectrum shows clearly that there exist cosmic rays with energies of at least up to 3×10^{20} eV. These highest energy particles must be extragalactic because they are too energetic to be trapped in our galaxy by the galactic magnetic field. So ν's and gamma rays at High Energies must exist because they are the ultimate decay products of interacting cosmic rays in the Cosmos.

Astronomy requires pointing back to the source, i.e. the origin of production. From the charged cosmic rays only those of the highest energies (probably protons) are not bent significantly by the galactic magnetic field. Therefore only a very low flux of cosmic protons are useful in pointing back to their origin. Neutrons are not very useful either, because only those with energies greater than 10^{18} eV live long enough to cross our galaxy. Unfortunately this flux is very low too. So, they cannot be helpful if their origin is outside our galaxy. Moreover protons (or heavier nuclei) with energies above 4×10^{19} eV interact significantly with the primordial 2.7 K microwave background. Their energy is rapidly degraded and eventually these particles generated at the highest energies get burried in the background of lower energies. So, charged hadrons cannot provide us informations for distances further away than 20–30 Mpc.

Observations of gamma rays with energies up to the tens of GeV [3] and the observation of Mrk421 (and Mrk501) with rays around 1 TeV [4] have stimulated calculations on the interaction of very high energy gamma rays with the ambient intergalactic photons [5, 6]. The calculations can be interpreted to show that the mean free path of gamma rays with energies above some hundreds of GeV is around 100 Mpc due to scattering with the intergalactic ambient infrared and ultraviolet starlight. This conclusion, combined with the calculations that show that attenuation due to scattering with the 2.7 K background is very serious for gamma rays with energies of hundreds of TeV, leaves the ν's as the only promising particles for TeV or Higher Energy Astronomy [7, 8].

Neutrinos not only go through interstellar space without attenuation but they also escape their progenitor's acceleration and target sites without absorption. Therefore the only way to measure the emission/production spectrum at the source is to measure the spectrum of the ν's arriving on Earth.

Relic ν's from the Big-Bang fill the Universe but no one has yet proposed a practical way to detect them. Low energy ν's of keV to $\sim$ 1 MeV are emitted continuously from the interior of stars like our Sun. At this moment there are several solar ν telescopes in operation, but there is no proposal to detect ν's produced in the interior of other stars. Slightly higher energy ν's ($\sim$15–20 MeV) are produced during the explosions of supernovae, as shown with the detection of supernova 1987A by KAMIOKANDE and IMB. But no practical way has been proposed to detect supernovae ν's further away than the immediate neighbourhood of our galaxy.

Neutrinos in the higher energies are produced from decays of particles produced from cosmic rays interacting and the subsequent cascades in the Earth's atmosphere. These Atmospheric ν's have a large energy spectrum, they become dominant above some tens of MeV.

Neutrinos with energies in the range of one to a few hundred GeV for example may also come from the annihilation of WIMPs in the Sun or the central core of the Earth.

Neutrinos from point sources are decay products of particles produced in hadronic interactions in potential cosmic accelerators such as neutron stars, black holes and young supernova remnants. Our own galaxy is full of such candidates. Further the Cosmos is full with Active Galactic Nuclei (AGN) and they are very

promising sources of Ultra High Energy ν's. Detection of ν's from point sources would unambiguously establish the existence of high energy hadronic interactions.

The physics aim of ν telescopes covers one or more of the following topics (in order of descending ν energy):

- Neutrino Astronomy (galactic and extragalactic) and the search for cosmic accelerators
- Physics beyond the Standard Model (Search for dark matter particles via their annihilation or decay to ν's, multiple W/Z production, search for possible substructure of the elementary particles)
- Neutrino oscillations using ν's produced in the atmosphere
- Long baseline ν oscillations using one of the high energy physics accelerators
- Proton decay
- Supernovae detection
- Magnetic monopoles
- The unexpected.

1.1 Production and detection of astrophysical high energy ν's

A recent review on the subject is given in [8]. According to [9], in optimal conditions for high energy ν production in a cosmic beam dump, a beam of 1 TeV ν's would be produced at a rate of 10% of the protons that strike the source. Under these conditions the ν flux emitted is at least 3 times bigger than the corresponding gamma ray flux produced by the same hadronic interactions. The photon interaction cross section is many orders of magnitude larger than the ν cross section, therefore high energy gamma rays can be destroyed much easier than ν's either near the source of their production by interacting with the matter or during their vast flight distance to Earth by interacting with the 2.7 K background or the infrared and ultraviolet starlight.

Another class of sources which has become rather popular in the last few years is ν's produced in the vicinity of Active Galactic Nuclei. In this mechanism, ν's originate from the decay of mesons which in turn are the decay products of photoproduced mesons. Recent calculations show that although signals from individual AGNs will not be detectable with the ν detectors presently under construction, the sum of all AGN's should be detectable.

Finally, we should mention that high energy ν's may also originate from heavy (hundreds of GeV) dark matter particles (or antiparticles) e.g., WIMPs which are trapped in the Sun or the Earth and which eventually annihilate producing ν's amongst other particles.

Neutrinos are detected by observing mainly the μ which is produced from the charged current ν interactions with matter, in the vicinity of the detector.

In high energy ν astronomy usually, it is not required to detect the vertex of the ν interaction, in this way one maximizes the available detection volume. The physics of the interaction is such that the angle between the detected μ and the parent ν direction [10] for 63% of the charged current events is $< 1.5^\circ/\sqrt{E\,(\mathrm{TeV})}$.

The decrease of the ν flux is partly compensated by the increase of the cross section ($\propto E_\nu$ until 10 TeV and then $\propto \log E_\nu$). Another parameter which improves with energy is the range of the μ ($\propto E_\mu$ until 1 TeV and then $\propto \log E_\mu$) and thus the effective detection volume of the detector is increased proportionately.

The signal to noise ratio increases with energy for the following reason. The inherent background comes from atmospheric ν's, which are the result of cosmic ray interactions in the atmosphere. The spectral index γ_ν of the flux of atmospheric ν's [11] follows that of the cosmic ray spectrum and is ~ 2.7 up to 100 GeV or so, but then at higher energies it becomes ~ 3.7, while ν's produced extraterrestrially follow the hard core ($\gamma \sim 2.0 - 2.2$) cosmic ray spectrum. So, for ν energies larger than 100 GeV the signal to noise improves with energy.

For all the above reasons it is advantageous to optimize the telescope for detection of high energy ν's. One should keep in mind though, that for very high energy ν's (e.g., from AGNs) the Earth is no longer transparent to ν's (e.g., the mean free path for a 500 TeV ν's is about one diameter of the Earth).

1.2 Backgrounds in Neutrino Telescopes

On the earth's surface the background due to the downcoming cosmic ray μ is overwhelming, the signal (for calculational purposes now we consider the atmospheric ν's as the signal) to noise (called up to down ratio) is of the order of 10^{-11}. Therefore, for shielding purposes, neutrino telescopes are located in deep mines inside mountains or in deep water. For instance, 4000 mwe (meters water equivalent) of shield reduces the up to down ratio to about 5×10^{-5} (Fig. 1) [2].

So, it is essentially impossible in the energy regime below 10 TeV to do neutrino astronomy by looking for downcoming μ's, because ν-induced μ's are indistinguishable from downcoming cosmic ray μ's. This is the reason that for those μ's which originate outside the detector (and therefore no vertex determination is possible) only μ's coming up from the lower hemisphere are useful.

Then the only remaining background is due to the omnipresent atmospheric ν's because the earth is transparent to them. In general, well shielded detectors can "look" up at about 20° *above* the horizon, while shallow detectors (1000 mwe) can look up only 20° *below* the horizon [12, 13, 14]. The kinematics of ν production and the multiple scattering is such that the best overall angular resolution is $\sim 1^\circ$. So in order to find point sources of ν's one would at best divide the sky into 1° square pixels. A source would manifest itself as standing above the background caused by the atmospheric ν interactions, which constitute a flat background (with

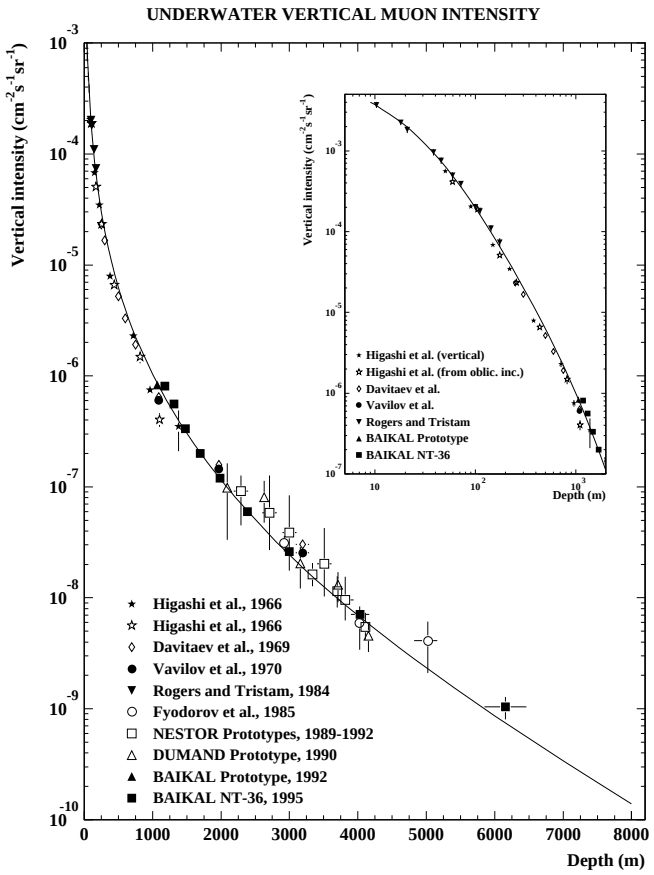

Figure 1: Vertical μ flux as a function of water depth.

a slight zenith dependence visible over tens of degrees).

Lastly, depending on the emission energy spectrum of the source, one can improve the signal to noise by demanding higher energy ν's (although Čerenkov detectors are very crude energy measuring devices).

2 Outline of the detector

The detector is located near the S-W of Greece a 8 km by 9 km horizontal plateau at a depth of 3800 m [15].

NESTOR deploys half of the phototubes looking upwards, thus having a 4π sensitivity and at the same time will be shielded by 3500 mwe. A total of 168 large 15 inch phototubes are employed. The basic detector element is a horizontal rigid hexagon of 16 m radius made out of titanium. At each one of the corners and at the center there is a pair of two 15 inch phototubes (one looking up and the other one down). By stacking 12 of these hexagons in the vertical, with a distance between hexagons of 20 m, we create a tower (fig. 2).

The effective area of a single tower for TeV μ's will be $\sim$ 20,000 m^2.

By deploying another six towers in a hexagonal fashion around the first tower and at a distance of 100–150 meters from it the array would have a sensitive area

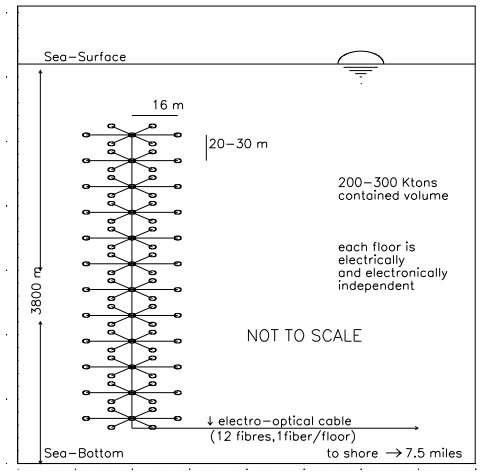

Figure 2: A NESTOR tower

larger than 10^5 m, it would provide an overall angular resolution better than 1° and it would have an enclosed mass of $>$ 20 Megatons. Within each one of the 7 towers the energy threshold is a few GeV, i.e. a low threshold active target of 1.5 Megaton mass.

3 Physics aims and detector sensitivity

3.1 Atmospheric Neutrino Oscillations

Results by the KAMIOKANDE, IMB and SOUDAN 2 collaborations [16, 17, 18] suggest that perhaps as much as 40 % of the atmospheric ν_μ events in the energy range from 0.2–1.5 GeV have oscillated to some other type of ν. Other, less sensitive but better shielded experiments did not record any effect [19, 20].

Assuming two flavor mixing (ν_a, ν_b), the oscillation probability is given by

$$P_{a\to b}(\Delta m^2, \sin^2 2\theta) = \sin^2 2\theta \sin^2(1.27\Delta m^2 L/E_\nu) \quad (1)$$

where $\Delta m^2 = m_a^2 - m_b^2$ is the difference of the squares of the mass eigenvalues in eV^2, θ is the two flavor mixing angle, L is the ν propagation length in km and E_ν is the ν energy in GeV. NESTOR can cover regions in the $(\sin^2 2\theta, \Delta m^2)$ plane which are not accessible to conventional experiments at accelerators or reactors. Moreover, it has a low energy threshold and can detect ν's of a few GeV, which makes it unique among the other underwater experiments. Given the rapidly decreasing atmospheric ν spectrum and the low energy threshold, NESTOR will accumulate enough statistics in a relatively short running time.

Eq. (1) shows that for a given value of $\sin^2 2\theta$ the lower bound of Δm^2 is proportional to E_ν/L. The search for ν oscillations using atmospheric ν's benefits from variations of ν paths through the Earth in the

range of 15 km to 13,000 km. Thus, due to the low energy threshold, we will be sensitive to an extremely wide range of Δm^2.

Due to limited statistics, most underground experiments can only detect ν oscillations by a change in the total ν flux, whereas in our case the possible existence of ν oscillation can be detected as changes both in the total ν flux as well as in the angular distribution, in the latter case independently of absolute normalization. Contained events or throughgoing μ's can be used.

3.1.1 Contained Events

These are events which have their vertex within the sensitive area of the detector (a cylinder with a radius of 16 m and a length of 220 m). The fluxes of the atmospheric ν's used for the present study (as inputs to the Monte Carlo) are those of [21]. In our energy range we have mostly ν_μ's and $\bar{\nu}_\mu$'s and a small fraction of ν_e's because at these energies cosmic ray μ's seldom decay in flight.

The integrated number of contained events expected in one tower – before any efficiency correction, for a year's running, above an E_ν threshold of 5 GeV is of the order of 2000.

The oscillation study is performed as a disappearance experiment by studying the zenith angle dependence of the flux. We look for differences between the number of downcoming ν_μ, which have the smaller oscillation lengths ($\sim$ 15 km), and the number of ν's coming from the sides or upcoming.

Due to symmetry in the zenith distribution around the horizontal and vertical directions in the absence of $\nu_\mu \rightarrow \nu_e$ oscillations the number of up coming should be equal to the downcoming. Any deviation from this equality will give indications of the ν_μ oscillations, which will be further enhanced by the so called matter effects for the $\nu_\mu \rightarrow \nu_e$ oscillations [22]; we are exploring a unique region in L and E_ν where these effects may further enhance the oscillation signal. They are due to the interaction of ν_e with the electrons in matter and are expected to be important only for path lengths of the order of the earth's diameter.

To perform this investigation we divide the range of zenith angles in six bins equally spaced in $\cos\vartheta$ (i.e. in $d\Omega$). The number of ν_μ in each bin has to be compared to the Monte Carlo calculation which includes the theoretical prediction [21] and takes into account the reconstruction efficiency obtained using events with a generated vertex within our sensitive volume. The number of cosmic ray μ's expected in a year's running for the three relevant angular bins is of the order of 10^7, whereas the number of expected μ's from atmospheric ν interactions is of the order of a hundred. Thus, we need a rejection power of about 10^{-5} in order to distinguish – in at least the first angular bins – the events due to ν's generated in the atmosphere from badly reconstructed events induced by cosmic rays. Note that in absence of oscillations the expected numbers will be equal for the symmetrical bins below the horizontal. The rejection power found by simulation, requiring μ tracks that start inside the detector, is 4×10^{-6} (preliminary). From the difference between numbers of events per bin for ν's with and without oscillation, we can obtain allowed/excluded contours in the $(\sin^2 2\theta, \Delta m^2)$ plane. The statistics allow us, after one year's running, to reach limits for the oscillations down to $\Delta m^2 > 3 \times 10^{-4}$ eV^2 and $\sin^2 2\theta > 0.3$ with a detector which is flux calculation independent and self-normalizable. Systematic uncertainties (e/μ identification power of our apparatus etc) are under study, but we know anyway that will be able to explore the KAMIOKANDE allowed region.

3.1.2 Upward muons

An alternative approach to the item of atmospheric ν oscillations can be provided by the measurement of the μ flux produced by atmospheric ν interactions in the matter surrounding the detector. The main disadvantages of this approach compared to the one of contained events are the relative high mean energy of interacting ν's which produce the flux of detectable μ's and the impossibility to distinguish between ν-induced μ's and atmospheric downward μ's. To avoid the latter effect we will restrict our attention to zenith angles greater than 85°. The reduction of the viewing angle will not allow to test the up-down symmetry for atmospheric ν's but a normalization of the absolute flux is still possible using the horizontal flux. The method is under study.

3.2 Celestial Point Sources

The extension of observational astronomy to very high energies gave birth to a new branch of astronomy, namely the Very High Energy and Ultra High Energy Astronomy and Astrophysics [23]). The observations of VHE and UHE γ-rays from celestial sources, point to the direction of highly energetic primary particles accelerated to these high energies. In isolated pulsars it is very well established that electrons are responsible for the observed high energy γ-ray emission. On the other hand, it is true that in general protons can be accelerated more easily to these high energies since they do not lose energy as easily as the electrons do through the inverse Compton effect and synchrotron radiation mainly. Objects that can accelerate protons to very high energies are expected, in addition to photons, to yield ν's as well, through hadronic interactions [24, 8]. Direct proof for the existence of protons accelerated to extreme energies are the cosmic rays that bombard the Earth.

3.2.1 The γ-ray data

In order to calculate the expected ν event rates for various objects we have to know the emitted high en-

ergy spectrum in each case. (Actually, this is what we will attempt to measure once the detector is operating). Therefore, we need an indirect estimate of the ν spectra for the various candidate sources. For this purpose we use the corresponding high energy γ-ray spectra.

In the past decades there have been reported VHE and UHE detections of various objects, although many of these detections are marginal. Most prominent among these objects are the Crab pulsar/nebula and the BL Lac objects Mrk 421 and Mrk501.

3.2.2 Calculation of ν Event Rates

The calculations were performed for one and seven towers and the results are given in table 1.

The optimum μ energy range at which we can look for point sources begins at the TeVs. Below 100 GeV the atmospheric background becomes strong and does not allow the detection of point sources. In the following paragraphs we discuss the results for each class of objects individually.

3.2.3 The Crab Pulsar/Nebula

This is an isolated pulsar embedded in an expanding shell of gas. It is the remnant of a supernova that went off $\sim$ 1000 years ago. We do not expect ν's from this object.

3.2.4 Mrk 421 and Mrk501

These are BL Lac objects (Quasars). Neutrinos are expected from these objects predominantly from $p\gamma$ interactions due to the intense radiation field. The expected event rates for Mrk 421 are lower limits due to the fact that while ν's escape freely once generated, γ-rays suffer attenuation in the source. We give rates for both the quiescent state and the active state of this object (the latest observations by the WHIPPLE observatory revealed a burst of activity ten times brighter [4]).

Mrk 421 and Mrk501 are the closest Quasars to the Earth at redshifts z = 0.031 and 0.034 respectively and the only ones observed at VHE γ-rays by the WHIPPLE group [4]. On the other hand, there are more Quasars observed in the MeV–GeV energy range by EGRET [3] brighter than Mrk 421 and with similar spectral indices (for example, 3C279 at its active state is $\sim$ 40 times brighter than Mrk 421), but which have not been observed at higher energies. This has been attributed to attenuation of VHE γ-rays from these objects through $\gamma\gamma$ interactions with the extragalactic starlight and infrared photons [5]. At the redshift of Mrk 421 this happens to photons with energy $E_\gamma >$ a few TeV, but the rest of the EGRET Quasars are much more distant, most of them at a redshift z $\sim$ 1. At this redshift, photons with energy greater than 100–200 GeV are attenuated significantly and this may be the reason that these Quasars have not been detected at VHE γ-rays despite the fact that they are brighter than Mrk 421. While this is true for photons, ν's do not suffer this attenuation and therefore NESTOR can expect to see more Quasars brighter than Mrk 421, especially when they are in their active state.

As an example, we give in table 1 the expected rates for the quiescent state of 3C273 based on model calculations [8] and the active state of 3C279 (extrapolated from the EGRET energy range since it has the same spectral index as Mrk 421). Other promising EGRET sources are 0208-512, 2251+158, 0235+164, 1633+382 [3].

3.2.5 The diffuse AGN background

Apart from point sources, another candidate celestial source of ν's is the diffuse AGN background. This is the combined emisssion from all AGNs which are distributed more or less uniformly all over the sky. The results are given in table 2 for four models of this background [25].

3.2.6 Event rate summary

The diffuse AGN background is the most promising candidate celestial ν source for NESTOR. Our calculations for the diffuse AGN background give appreciable event rates in the TeVs (hundreds to thousands events/yr) even for one tower ($\sim$ 20000 m^2). On the other hand, the calculations for the point sources for 7 towers ($\sim$ 100000 m^2) give lower limits to the expected event rates in the range: 1–400 events/yr. The corresponding event rates drop by a factor of 3 for one tower. Among the point sources, individual AGN at their active state are the best candidates (many tens of events per year). The bright bursts of X-ray binaries are a good possibility too, since in this case we expect to see a minimum of $\sim$ 4 events in the course of a few hours. A very prolonged active state of the X-ray binaries would yield a much higher yearly event rate but it is not very likely that these objects can stay in the high state for periods as long as a year. The above numbers came from the γ-ray fluxes and we did not take into account any attenuation of the photons in the sources.

As we saw in the previous section, the ν fluxes can be higher by one or even two orders of magnitude under favorable conditions and in this case a single tower would be able to detect a few point sources.

3.3 Indirect Detection of Non Baryonic Dark Matter

An indirect method of non baryonic dark matter detection [26] consists in detecting ν's produced by their annihilation in the core of astrophysical objects. Neutrino telescopes which are sensitive to ν's with energies above 5–10 GeV are particularly well suited for this purpose.

In the MSSM (Minimal SuperSymmetric Standard Model) the supersymmetric partners of the neu-

Object	Stage I (1 tower) (> 1 TeV) – (> 10 TeV)	Stage II (7 towers) (> 1 TeV) – (> 10 TeV)
Mrk 421	0.4 – 0.3	1.3 – 1.1
" (active)	2.0 – 1.7	7.0 – 6.0
3C273	3.0 – 2.5	8.0 – 6.5
3C279 (active)	16 – 12	53 – 42
XRB bursts	1.1 – 0.8	4.0 – 3.0
Atmospheric	2.0 – 0.14	0.6 – 0.04

Table 1: Expected number of events per year for the point sources (lower limits). For the XRB bursts the numbers are events/burst. The resolution for a single tower is 5° while for the 7 towers it is 1°.

Model	Stage I (1 tower) (> 1 TeV) – (> 10 TeV)	Stage II (7 towers) (> 1 TeV) – (> 10 TeV)
Protheroe	13500 – 10800	40000 – 32000
Sikora	760 – 690	2000 – 1970
Biermann	280 – 220	750 – 640
Stecker	120 – 120	380 – 380
Atmospheric	1500 – 120	4000 – 420

Table 2: Expected number of events per year for the diffuse AGN background.

tral bosons are four neutralinos: the two partners of the neutral SU(2) and U(1) gauge bosons (gauginos), $\tilde{W}_3$ and $\tilde{B}$, and the two partners of the neutral Higgs particles (higgsinos), $\tilde{H}_1^0$ and $\tilde{H}_2^0$. The lightest neutralino is a linear combination of photino ($\tilde{\gamma}$), zino ($\tilde{Z}$) and higgsinos ($\tilde{H}_{1,2}^0$).

3.3.1 The Neutrino-Induced Flux

Neutrino telescopes would be sensitive to ν's produced in the annihilation of neutralinos captured in the core of astrophysical objects like the Sun and the Earth.

The neutralinos move in the halo of the Galaxy with velocities of few hundreds of km/s and loose energy by elastic scattering on the nuclei forming the matter of the Sun or of the Earth when they cross them. The escape velocity is 11.2 km/s at the Earth surface and 617.5 km/s at the Sun surface. Since neutralinos have typical velocities of ≈ 300 km/s they are captured by the Sun quite efficiently, while the probability that they are captured by the Earth is smaller unless their mass closely matches the mass of an element abundant in the Earth. Due to the energy loss the neutralinos accumulate to the core and, then, they annihilate by pair. The subsequent decay of particle produced in the various final states would generate a flux of high-energy ν's.

A description of the mechanism has been done by many authors [27]. Calculations performed by Bottino et al. [28] show that due to the age of the solar system ($t_\odot = 4.5 \times 10^9$ yr) the equilibrium between the capture and the annihilation is reached for the whole range of m_χ, whereas for the Earth the equilibrium conditions depend on the values of the model parameters.

3.3.2 The Sensitivity of a Generic Detector

Neutrinos are detected either using contained events where the charged-current interaction νN produces a lepton in the detector or using upward-going μ's produced by $\nu_\mu N$ charged-current interactions in the medium surrounding the detector. The cross section for a charged-current interaction is proportional to the ν energy and the range of a μ is proportional to the μ energy. The rate for contained events is, thus, proportional to the ν energy and the rate for ν-induced throughgoing μ's is proportional to the square of the ν energy. Therefore at high energies the detection of ν's results to be more efficient by using throughgoing μ's than by using contained events. This is the reason why we will concentrate on this method of detection.

Due to large variations of the S/B ratio the detector sensitivity strongly depends on the neutralino mass hypothesis. The sensitivity may be defined as the minimal exposure $(At)_{\rm min}$ necessary to see a 4σ effect (with a signal of at least 4 events). This quantity has been estimated in Ref. [28] for neutralino annihilations in the Earth core. A very low value of $(At)_{\rm min}$ is necessary ($\simeq 50\,{\rm m}^2$ yr) for a neutralino mass value around the iron nucleus mass, but exposures above $10^4\,{\rm m}^2$ yr are necessary to detect masses above 100 GeV.

The minimal exposure necessary for neutralino annihilations in the Sun has been also calculated. With the exposures that can be reached with the detectors operating today ($\simeq 10^3\,{\rm m}^2$ yr) only neutralino annihilations in the Earth can be explored in the mass range 50–100 GeV. The exploration about neutralinos using the flux from the Sun requires at least $10^4\,{\rm m}^2$ yr. The next generation detectors would provide exposures larger than

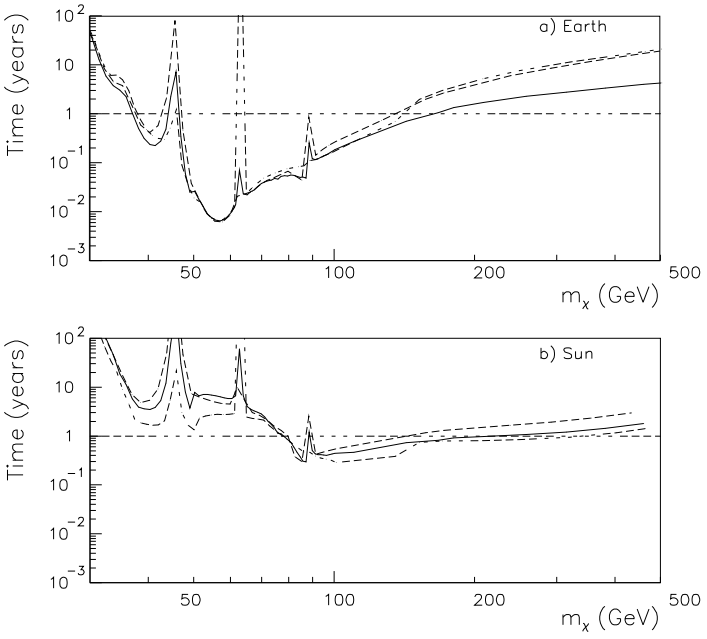

Figure 3: Minimal exposure time necessary to detect a 4σ effect with one tower as described in the text. Figure (a) refers to a signal coming from the Earth core and figure (b) is for ν's from the Sun. The three neutralino compositions are $P = 0.1$ (dotted line), 0.5 (solid line), 0.9 (dashed line).

10^5 m^2 yr allowing the simultaneous exploration of neutralinos using both the ν fluxes from the Earth core and from the Sun in the range 35 GeV $< m_\chi <$ 500 GeV.

The predictions given above depend sensitively on several free parameters.

3.3.3 The Sensitivity of One NESTOR Tower

The exposure time necessary to detect a 4σ effect from the Earth core and from the Sun with one tower has been estimated. Fig. 3 shows the minimal exposure times as a function of the neutralino mass m_χ. This figure shows that in one year of running time one tower could detect neutralinos with masses in the range 50–140 GeV from the Earth core and with masses in the range 80–200 GeV from the Sun.

3.4 Long Baseline Oscillations with CERN

The probability for two flavor ν oscillations is given by Eq. (1). As a simple rule the minimum statistical sensitivities for the mixing angle θ and for the difference of the mass squares Δm^2 are given approximatively by the formulae [29]:

$$P_{\min} = \sin^2 2\theta_{\min} \sim \frac{\sqrt{N}}{N}, \qquad (2)$$

$$\Delta m^2_{\min} \sim \sqrt{P_{\min}} \left(\frac{E_\nu}{1.27L} \right) \text{ eV}^2, \qquad (3)$$

where N is the number of detected events, L is the ν propagation length (in km) and E_ν is the ν energy (in GeV). Thus, in order to maximize sensitivity, it is necessary to have the longest possible base-line and lowest threshold energy whilst detecting sufficient ν events for statistical significance.

Two accelerator experiments, CHORUS [30] and NOMAD [31], looking for ν_τ appearance at larger Δm^2 in the present CERN wide-band ν beam are currently taking data; first results are expected in 1995-96. Clearly one would like to continue with controlled beam experiments because they have the following advantages over the atmospheric data:

- Initial flavor composition is well known (typically $\nu_e/\nu_\mu \sim 0.01$).
- Control of the beam polarity. One can switch between ν and $\overline{\nu}$ to study matter enhanced oscillations (MSW effect [32]).
- Control of the energy. One can typically obtain beam energy dispersions σ_E of about 5 GeV.
- One may specify the direction cosines and time of arrival of the ν, improving efficiency and reducing backgrounds to almost zero.
- Higher statistics, giving sensitivity to lower mixing angles.
- Control of the beam energy which provides a way to differentiate between oscillations from ν_μ to either ν_e or ν_τ.

In NESTOR, a complementary study to the atmospheric ν oscillation can be conducted with a long baseline experiment with a CERN beam. As part of the work on the LHC, injection transfer lines are being designed to bring the fast extracted beams from the SPS to the new collider. The primary proton beam for a ν production target to feed Gran Sasso with only minor modifications can be derived from TI48 which links SPS/LSS4 to LHC/P8. On a two dimensional projection CERN, Gran Sasso and NESTOR are lined up. Calculations by Mayoud (CERN) show that a ν beam pointing to NESTOR would have to be diverted by only 1° to the west in azimuth and 5° or 7.5% downwards in declination, with respect to the one pointing to Gran Sasso.

For the latest long baseline beam design for NESTOR [33] with a horn and a reflector, for a 450 GeV beam, the lateral beam spread at the NESTOR site is flat to $\pm$ 2.0 km around the target point, so targeting should not be a problem. We calculate that for 10^{19} protons on target a 200 kt detector e.g. one tower should detect about 15 thousand contained events.

Such an experiment will require more photomultipliers per tower and more than one tower appropriately configured to enhance e/μ separation. The separation of μ from e and hadrons in such a detector is under

study. Preliminary MC results indicate that it will be possible to distinguish between "muonless" (NC) and "muonfull" (CC) events, by using the time distribution of the events (Čerenkov light from μ's comes earlier than the one from the hadronic or electromagnetic showers) and the longitudinal shower development of the event (the μ's distribute their Čerenkov light evenly while electrons emit their light according to the development of the electromagnetic shower). The systematic effect due to this statistical separation is estimated to be of the order of 10 %. The CERN ν beam produced by the 450 GeV SPS beam with horn and reflector, targeting NESTOR will produce the sensitivity required to explore the Kamiokande allowed region in one year's running (10^{19} protons on target). It will cover the area of small mixing angles, due to better statistics, provided that we will be able to control the systematics.

4 The detector

Among the detector's specifications, some of them, like the effective area to be covered, the angular resolution for the single μ produced in the water, the granularity (i.e. the spacing of the PMT's related to the sensitivity of the light detectors) and the water transmissivity length, play a very important role to define the physics potential of the apparatus. A certain flexibility to change the detector geometry and to upgrade it, is also important. Finally the overall costs, including the costs of the materials, the deployment and the servicing also must be taken into account in order to be kept as low as possible.

NESTOR's physics goals range from atmospheric ν oscillations (of a few GeV) to Very High Energy ν's from Extragalactic sources (at least 1 TeV).

We will start with a detector of a sensitive area of 20.000 m^2, expanding it in a modular fashion to 100.000 m^2 and hopefully later to the 1 km^3 detector which is probably required to detect point-like sources, given the expected ν fluxes. The Monte Carlo calculations indicate that a very favourable geometrical symmetry to cover 100.000 m^2 (which is probably the minimum area required to start point source astronomy) is a cylinder of an enclosed mass greater than 20 Mtons and overall angular resolution better than 1°.

The Optical Module consists of a photomultiplier tube (PMT) inside a high pressure glass housing sphere. The PMT is glued to one hemisphere using an optically transparent silicone gel which provides good optical coupling. To minimize the geomagnetic field inside the tube, the PMT is surrounded by a mu-metal mesh. The sphere contains also the PMT high voltage supply. No other electronics are contained in the Optical Module. The current design of the detector assumes the use of omni-directional units consisting of two back to back optical modules each containing one PMT. The 15 inch Hamamatsu R2018-03 was selected. Six pairs of PMT's will be placed at the corners of a horizontal hexagon and a seventh one in its center. The radius of the hexagon is planned for 16 m, and the arms made out of titanium piping. The electronics (data digitization/transmission to shore) and all the controls of the hexagon will be housed inside the titanium sphere located at the geometrical center of the hexagon.

By stacking hexagons we can build "towers". The vertical distance between these hexagonal floors will be around 20 m, this spacing matching well the light transmission length of 55 ± 10 m (at 460 nm) that we have measured (see previous chapter). With a 20 m vertical spacing between floors, each with 7 phototubes looking up and 7 phototubes looking down, the active volume between hexagonal floors will be monitored efficiently. A total of 12 such hexagonal floors is planned for one tower. The mechanical design is an extension of the hexagonal autonomous module with rigid arms made up of an assembly of thin Ti tubes, that we used during the tests off Pylos in the summer of 91. Other designs, materials and deployment techniques are also under consideration.

5 Deployment

Various deployment procedures are under study, appropriate to the proposed mechanical designs.

The deployment procedure that has been considered for the mechanics design described above avoids the use of bathyscaphs for connections in the sea. A vessel (barge) will carry the floors in their folded position. The weight platform with the anchor release will go into the water first, followed by the Fan-Out titanium sphere which will have the main connection of the undersea power and optical cable and the power and optical connections for each floor. Before each floor is immersed into the sea, the electrical and optical connections will be made. Then the tower will be lowered to the bottom of the sea with the help of the weight of the anchoring platform and 4 km long steel wire cable. The first tower will be positioned very roughly at the center of the basin. The next six towers will have to be positioned around the first one at a distance of 150 ± 10 meters. This can be accomplished with the use of the existing technology.

We are in collaboration with specialized firms for consulting e.g. IFREMER, TECNOMARE, COMEX, GKSS, that can provide us with expertise on the mechanical structure, reliability issues, materials to use, connectors, buoys, deployment, positioning (sonars and GPS), bathymetry, sedimentology, video monitoring etc.

6 Positioning

The expected deviation from the vertical of the tower depends on the undersea water currents which have been measured to be under 10 cm/sec. Depending on the strength of the currents the axis of symmetry of

the tower will not necessarily be a straight vertical line but occasionally it may be parabolic, catenary. The exact location of the optical modules has to be known to within a few tens of cm in order to reconstruct the μ track direction accurately (to within 1°). The continuous recording and monitoring of these positions will be accomplished by a chirped sonar system which is controlled by the Slow Controls System. This acoustic system consisting of a set of transducers (responders) will be located at positions a few hundred meters around the tower and will emit, when commanded from a central control, frequency modulated acoustical signals (chirps) which will be detected by hydrophones located at each floor. The distance of the optical modules from the hydrophones is known because the hexagon arms are rigid. Their coordinates will then be determined via triangulation. Parameters like pressure, temperature and salinity of the environment which influence the speed of sound in the water will be recorded by the Slow Controls System.

Each responder unit is a combination of a pinger and a hydrophone and it is acoustically interfaced to the Slow Controls System. We will use commercial responders and hydrophones. The responder units are battery powered and will be dropped at distances of about 200-300 m around the tower at deployment time. They typically have a battery life (lithium batteries) of several years and will respond for 10^5 pulses after which we can recycle them. They will respond to acoustic commands sent by one of three transponders located close to the bottom of the tower and controlled by the Slow Controls system. The response will be the emission of acoustic chirps which will be detected by the hydrophones. The differential time between floors will give the curvature of the tower and the timing with respect to the transponders will give the relative position of the tower. The use of a surface ship with differential GPS (precise satellite navigation) will yield the absolute location at the responders to $\pm$ 1m. The relative PMT positions will be determined to within 10 cm.

In addition to the acoustical data there will be information from the compasses and the tilt meters. This information will be correlated with the acoustical information and provide a redundancy in the determination of the physical shape of the tower.

7 Data transmission

Each floor will have its own electronics, monitoring and controls housed in the titanium sphere at the center of the hexagon.

The signals for all fired PMT's will be transmitted over a distance of 25 km. We want to be able to transmit to the shore laboratory, in real time, the complete pulse of each PMT signal, maintaining the time coherence between PMT's. This feature of the data transmission, that distinguishes NESTOR from the other ν telescopes, has many advantages:

- real time control of the behaviour of the single PMT during the data acquisition
- trigger logic decided on shore (maximum flexibility)
- the knowledge of the pulse shape.

The last point could be very helpful to distinguish different physics events. The pulse shape is expected to be μ energy dependent for energies greater than about 100 Gev and to be also different in events with more than one μ, for which the pulse shape will play a crucial role in their identification. MonteCarlo calculations of these effects are in progress.

The transmission method of the PMT pulse shape on the optical fibre is strictly related to the characteristics of of submarine multifibre optical cables that are commercially available. If a 200 fibres submarine cable were affordable the signal transmission could be achieved with one fibre per phototube. In this case a simple solution, in order to have a high (> 10 *years*) Mean Time Between Failure (MTBF), would be to provide each PMT with one laser and to modulate with the anode current the light power of the laser.

The collaboration have investigated a possible transmission method based on a 12 or 18 fibres submarine optical cable at present available (ALCATEL, ATT, PIRELLI etc). With such a cable the use of one fibre per (at least) one plane is mandatory: signals from the 14 PMT of each plane are first multiplexed and then transmitted on one single fibre. The data of the whole tower are transmitted in 12 fibres.

Different methods have been examined:

1. digitization and time multiplexing
2. transmission of the analog signal with either a) amplitude modulation and frequency multiplexing or b) frequency modulation and frequency multiplexing or c) wavelength division multiplexing

The first one has been retained by the INFN group and is in the most advanced state. The collaboration will probably choose this one as the main option.

7.1 The digital transmission scheme

In this scheme the signal of a PMT is sent to the Titanium sphere at the center of the floor, which contains the electronics for the 14 PMT's. The signal is first sampled with a Flash A/D, then multiplexed together with the signals of all the PMT's of the same plane. The multiplexed signal modulates a laser and the light output is sent by an optical fiber to the fan-out sphere where 12 fibers enter the electro-optical cable. The PMT pulse data are transmitted only when the result of the digitization is over a certain threshold. The transmission contains the A/D samples together with the time when the PMT pulse amplitude crosses the threshold (threshold time, further on also referred to as "event time") and pulse information. The synchronization between

signals of different PMT is assured from the transmission of a unique Master Clock signal from the shore to the 12 planes and from a synchronous answer sent from each plane to the shore. This allows also a correlation of the PMT event time with the on shore time.

On shore the data of each PMT collected in a time window of 6144 μs, periodically cleared, are memorized in a RAM (data RAM). Moreover the event time and the charge are extracted from these data and used from a dedicated processor ($DECPerle_1$) to build a first level trigger. Once the trigger condition is met, the full PMT data collected in the data RAM are read using the event number as memory address.

7.2 The analog transmission scheme

The transmission by optical link of the analog signals of the PMTs has the powerful advantage of leaving a complete flexibility for the subsequent processing of these signals on shore.

The use of single frequency laser diodes, usually distributed feedback (DFB) laser diodes, is required in order to transmit through a 25 km optical fiber the R2018 PMT signal which has a 8 ns rise time.

We have considered direct or external modulation of the laser diode.

7.2.1 Direct modulation

In order to comply with the available optical cables and to minimise the number of the DFB laser diodes one has to rely on multiplexing, i.e. transmitting into one fiber several signals by modulating a common optical device. Frequency (RF) Division Multiplexing (FDM) or Wavelength Division Multiplexing (WDM) are possible.

The RF modulation can be either amplitude modulation which minimizes the required laser frequency bandwidth at the expense of a reduced dynamic range, or frequency modulation with the complementary drawback and advantage. A reasonable design which also matches the number of fibers in commercially available optical cables consists in FDMultiplexing the 14 channels to modulate one DFB laser diode per floor. Each PMT signal modulates an oscillator output and the 14 resulting signals are combined to modulate the laser. Oscillators have to be in the immersed detector since any solution with oscillators on shore will require additional lasers and photodiodes as well as multiplexing systems. The carrier frequencies should be such that the first harmonics are outside of the useful frequency range. Direct modulation of laser diodes is a solution which is currently used for cable TV applications. We are constructing a 3 channel prototype for a frequency modulation multiplexing in order to evaluate the feasibility of a system associated with a 10 GHz DFB laser.

7.2.2 External modulation

External modulation has in principle the advantage of allowing the laser to be on shore. Mach-Zehnder modulators utilise incident polarised laser light and their use has been discarded. Asymmetric Fabry-Perot (multi-quantum well - MQW) modulators are used in an infrared link under development by the CERN DRDC Project RD23 [37]. With this system, an infrared laser beam is generated on the shore and is guided with a single-mode fiber to a reflective modulator. The analog signal of each photomultiplier modulates the reflected light intensity and an infrared detector on the shore reproduces the analog signal.

7.3 The electro-optical cable

The transmission of the signal over 25 km forces the choice of the single mode (or monomode) optical fibre and of a laser as light source. Power transfer to the tower and data retrieval to the shore will be performed with an electro-optical cable. For the data transfer and the telemetry support we will use the standard deep sea electro-optical telecommunication cable. It is composed of (at least) 12 monomode optical fibers, one for each floor. The fibers are located inside a plastic core and they are surrounded with a copper conductor, which delivers the required power for the operation of the tower (as power "return" the sea water path will be used). The cable will be attached to the tower and all electrical and optical connections will be made in air before tower deployment.

8 Trigger and Data acquisition

NESTOR will be sensitive to ν's that range from the TeV scale, e.g ν's coming from Active Galactive Nuclei (1 per day), to atmospheric ν's (GeV scale) or ν's coming from neutralino annihilation (a few per day), and should be able to record hit multiplicity fluctuations in order to detect a signal of Supernovae explosions, or very slow heavily ionizing particles (monopoles). Further it should record the downcoming cosmic ray μ background ($\sim$1 Hz) which will serve as calibration of the detector. Table 3 shows the expected number of physical events that will occur in the detector per day.

The natural background to the photomultiplier tubes (PMT): bio-luminescence and natural sea radioactivity, ^{40}K, gives a initial high counting rate ($\sim$ 50 kHz/PMT, maximum 100 kHz/PMT) that has to be reduced down to the few Hz level through a series of trigger decisions of increasing complexity.

Table 4 shows the expected number of double triple etc. coincidences due to the above accidental background expected in one tower. For the higher level coincidences the time-coincidence window depends on the actual distance of the PMT's hit, and some causality criteria have been applied. This is the ideal situation, assuming large computing times. A fixed-gate coinci-

Process	1 tower	7 towers
AGN ($\geq$ 1 TeV)	0.5-1	1-2
Atmospheric throughg. ($\geq$ 1 TeV)	4-5	10-12
Atmospheric contained	2	14
Atmospheric upcoming μ	1.5	10
χ upcoming μ (earth) m_χ=56 GeV	5	35
χ upcoming μ (earth) m_χ=100 GeV	1	7
χ upcoming μ (sun) m_χ=100 GeV	1	7
Cosmic ray downcoming μ	86500	600000

Table 3: Expected events per day from main physical processes

Noise Frequency	50 kHz	100 kHz
singles	8400	16800
doubles	537	1500
triples	18	78
quadruples	.5	4

Table 4: Random coincidence rates in kHz

dence scheme that was simulated gives larger rates. The required data transmission rates lead us to go above the four-fold coincidence level in order to transmit realistic dataloads, of a few MB/s, to the next level of triggering.

The field programmable gate array technique is a very good candidate for a first level trigger due to its low latency [3] and essentially through its flexibility to be rapidly and simply reconfigured, since the trigger will have to adapt to changing environmental conditions, and physics interests. From then on the computing power of processors with high-level languages (e.g alpha) or farms of processors will be adequate to treat the data.

From the trigger point of view, NESTOR presents, as can be seen from the above tables, similarities with LHC experiments (after their 1^{st} level).

8.1 Data Rates

The raw data rate is dominated entirely by the background pulses. The time and charge profile (sampled with a 300 MHz FADC on the PMT analog output) will be transported with optical fibers to shore, every time a PMT gives an output larger than a threshold (e.g .25 of single photoelectron).

The signals from the whole detector will be fed in the 1^{st} level trigger processor with a frequency of 20-25 MHz. The goal is that the 1^{st} level trigger processor will reduce the rate below the kHz level, and thus it will reduce the data rate from an average 320 MB/s (maximum 640 MB/s) down to a few MB/s. The event building, will be done by the 2^{nd} level processor collecting 1-2 μs worth of information from the 12 floors. At the 2^{nd} level a single processor (e.g an alpha) or a farm of processors connected with point-to-point links (e.g SCI) or ATM switches can perform high level fits to reduce the event rate down to a few Hz.

[3] time needed to make a decision in a pipeline environment

8.2 1st level trigger

DECPeRLe$_1$ is a Programmable Active Memory [38], a novel form of universal hardware co-processor based on *Field-Programmable Gate Array* (FPGA) technology and controlled by a general purpose computer system. It is a single board system housed in a desktop workstation enclosure. The computational core of DECPeRLe$_1$ is a 4 by 4 matrix of Xilinx XC3090 FPGAs [39] connected in a regular mesh.

The computational challenge of the first level trigger is to detect correlated pulses from several PMTs due to Čerenkov photons emitted by tracks traversing the array against a backgound of random uncorrelated PMT firings. The distance between PMTs places a strict upper bound on the time difference between pulses that may be correlated. For neighbouring PMTs this is $\sim 100ns$. These events need to be distinguished from randomly correlated pulses among groups of PMTs, due to background fluctuations.

We need to detect from double to multiple coincidences and then apply a weighed sum to all coincidences found in a given time window. When correlation scores exceed a given threshold associated data will be passed to the reconstruction process.

A simple trigger algorithm based on the total number of p.e.'s has been tested with signal events (1 to 50 GeV contained μ's, pointing at random directions) and noise. The efficiency of the algorithm and the noise rate as a function of the number of photoelectrons (p.e) required are shown in table 5.

Trigger	Noise rate kHz	Muon Efficiency
3 p.e	40kHz(100)	-
4 p.e	8(30)	-
5 p.e	2(10)	100%
6 p.e	0.3(5)	98%
7 p.e	$\leq$0.1(1)	96%
8 p.e	$\leq$0.1(0.3)	94%
9 p.e	$\leq$0.1(0.2)	92%

Table 5: Noise rates for the whole detector in kHz under the assumption of 50(100) kHz singles rate/PMT and efficiency for contained μ events from 1 to 50 GeV, normalised to the requirement of at least 5 p.e.

8.3 2^{nd} level trigger and DAQ

One should expect of the order of 1-5 MB/s of data with a frequency between 2 and 10 kHz, to be transmitted to the data acquisition workstation. A relatively simple and fast algorithm written in a high language could reduce further the event rate by using a "pre-fit" to

less than a hundred of Hz. We estimate that one alpha workstation of the high end should be able to cope with the rate. In the case that more computing power is needed, e.g in the case of unexpectedly high noise, the system is easily upgradable to a small farm of alpha workstations. This scheme concerns only one tower. In the case of more towers one should go to a mutiprocessor environment with fast point to point links of the type SCI, or ATM switches.

9 Slow control, calibration and positioning

The Slow Control System is responsible for a variety of tasks:

- The control of the power distribution to the twelve Ti Spheres (one per floor) and to the single photomultiplier tubes (PMT).
- The control of the threshold settings for the PMT discriminators.
- The readout of the internal and external environmental monitors.
- The control of the LED calibration system.
- The control and readout of the positioning system hydrophones.
- The communication between NESTOR and the associated experiments (Geology, Oceanography, Marine Biology, etc.).
- The communication with the shore station for readout and command transfer.

Central to the Slow Control System is the general NESTOR philosophy that failure of a particular component should not impair the performance of the rest of the experiment. The items controlled by the Slow Control System are:

Per floor: measures of internal temperature, humidity, tilt, orientation (with compasses), pulsers, control of PMT power, thresholds.

General: measures of external temperature, pressure, sea current, salinity, control of power to floors, releases.

The components of the Slow Control System in the twelve Ti Spheres, the Transmission System, the Fan-Out Sphere and the Shore Master Control are described below.

9.1 The Ti Spheres and the Transmission System

.

The twelve Ti Spheres (one per floor) contain the bulk of the electronics. Every sphere contains the PMT transmission electronics board, which also receives from shore the synchronization signals. The bandwidth (1 GHz) is so large that the data from/to the Slow Control System can fit easily in the PMT transmission frame. The communication between the Slow Controls board and the PMT transmission board will be implemented via a RS/232 asynchronous link, with a minimum of interference to the fast PMT transmission electronics. The Slow Control board will be an intelligent board based on a microcontroller with several I/O channels. RS/232 and ADCs will be used to communicate with the different sensors envisaged. Solid state relays will turn the 24 V power on and off to the 14 DC/DC converters housed in the Benthos Spheres which will generate the high voltage for the 14 PMTs of a floor. A voltage divider will set the appropriate voltage for every PMT.

9.2 The Fan-Out Sphere

The Fan-Out Sphere, located below the tower, is responsible for the power and fiber distribution to the Ti Spheres in the center of the 12 floors. A lot of attention has been devoted to this sphere because it is essential to the entire experiment. The Fan-Out Sphere is a Titanium sphere which contains:

- the optical fiber splice that will separate the twelve fiber cable into twelve individual cables, one per floor
- a power distribution system with one cable for each of the 12 floors. It will be possible to switch the 300 V power on and off to the individual floors. A parallel system involving slow modem transmission on the power cable from the shore is being investigated to have a more robust system.

The Fan-Out Sphere will be filled with oil to prevent any possible water leakage.

9.3 The Shore Master Control

The Shore Master Control includes:

- The control computer, running preferably under LabVIEW.
- An interface between the computer and the VME crate where the transmission electronics will collect the data from the PMTs.

It will be the responsibility of the transmission electronics to extract from the PMT data stream the Slow Controls data and to put them in a separate area of memory, from where the Shore Master Control will recover them for storage and display. The system could also be very useful to snoop on the PMT data while they are being examined by the trigger system.

9.4 Reliability

Reliability is the focal issue. The electronics will be underwater and it will be impossible to service it if any problems arise. Therefore the components of the system have to be chosen with reliability as the primary objective. This means not only choosing MIL specs components, but also minimizing the number of

parts and designing in a fail safe fashion. Duplication of functions will be used wherever possible. It is however necessary that a whole system analysis be carried out before the final design is implemented, including failure mode studies and parallel processing issues.

10 Detector response

10.1 Signal Simulation

The expected signals arise from a large variety of events : single and multiple μ's coming from any direction with energy ranging between few GeV and PeV or more; ν's with the same energy range which can produce μ, electromagnetic and hadronic showers at any point of the detector. Moreover μ bremsstrahlung, direct pair production and photonuclear cross sections increase with energy together with the production of energetic δ rays and each charged particle created along the μ path contributes to Čerenkov light. As a consequence the light emitted by a very high energy μ behaves very differently from the simple light cone emitted by a single charged particle.

10.1.1 Photoelectron production and detection

The mean number of detected photoelectrons (P.E.) is a function of the radial distance (i.e. the distance of closest approach) between the track and the PMT (at the NESTOR site the water transparency is equal to 55 meters). At 10 m, for example, 5 p.e. are detected in average from the primary track, not including the emission of Čerenkov light from secondaries.

As the μ energy increases, the fluctuations of the number of photoelectrons around the mean value increase drastically as a result of the large fluctuations which characterize the generation of secondaries by the μ. The increase of the tail in the distributions is the major factor in the increase of mean P.E. number with energy. Fig.4 shows the probability distribution of the number of photoelectrons, detected by one PMT, produced by the photons emitted from a μ track at two different energies at a radial distance of 18 m from the PMT. The area under each curve is normalized to 1.

The photons coming directly from the μ arrive within a time interval of about $2ns$ but a small amount of photons coming from electromagnetic showers around the μ arrive later because they are emitted, with respect to the μ direction , at an angle different from the Čerenkov angle Θ_C. The amount of such delayed photons increases with the energy of the μ due to the increase in the number of electromagnetic showers around it. Fig.5 shows the probability distribution for the P.E. arrival time. The arrival times are smeared with a Gaussian spread ($\sigma = 2.5$ ns). The signal comes from a μ track at a radial distance of 18 m from the PMT.

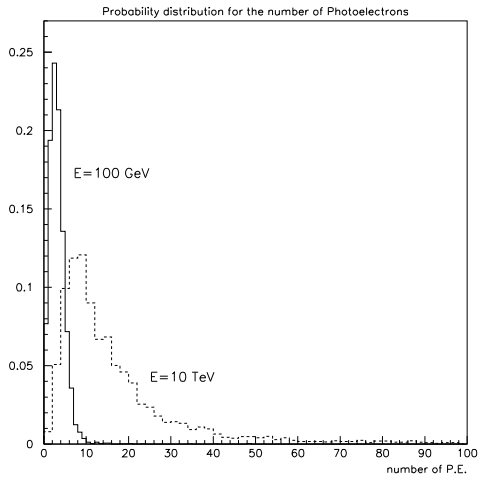

Figure 4: Distribution of the number of photoelectrons detected by the phototubes for μ's with 100 GeV and 10 TeV energy.

10.2 Low energy muon and electron reconstruction

We aim to reconstruct and recognize low energy electrons and μ's generated within the geometrical volume of our detector and to try to discriminate between the two types of events. The electron reconstruction algorithm is based on the fact that the electron will shower within a few radiation lengths from its generation (x^o=36 cm). In order to distinguish between μ's and electrons in an event we perform a "muon hypothesis" and an "electron hypothesis" fit. We apply cuts on the χ^2 of the two fits. We then apply cuts that take advantage of the differences between the two processes: for an electron we require that most of the charge be localized within a couple of detector floors, whereas for the μ that it be more or less evenly distributed along its path. We cut also on the maximum angle α_{max} formed between the lines joining a pair of hit PMT's and the reconstructed pseudovertex, because the vast majority of the μ photons come from Čerenkov emission and the angle α cannot be more than $2 * \Theta_C$, whereas for the electrons α_{max} is much wider. With these criteria we get for 12 Gev electrons and μ's roughly 60% reconstruction efficiency and 5% misidentification.

10.3 Low energy contained ν interaction

The reconstruction of the interaction of a low energy ν that interacts within the geometrical volume of our detector is a complex problem. Two dedicated codes to handle these events are at the development stage.

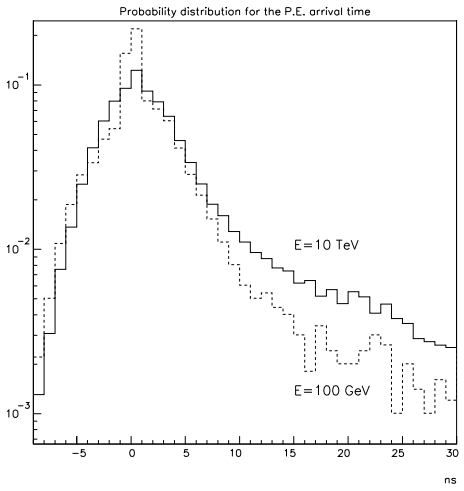

Figure 5: Distribution for the P.E. arrival time

10.4 High energy muon reconstruction, effective area

We show in figure 6 the effective area for 1 TeV μ's and 10^o reconstruction accuracy as function of $cos\theta$ (zenith angle) and in figure 7 the effective area averaged over all angles as function of the μ energy, for μ energies from 0.1 TeV to 1000 TeV.

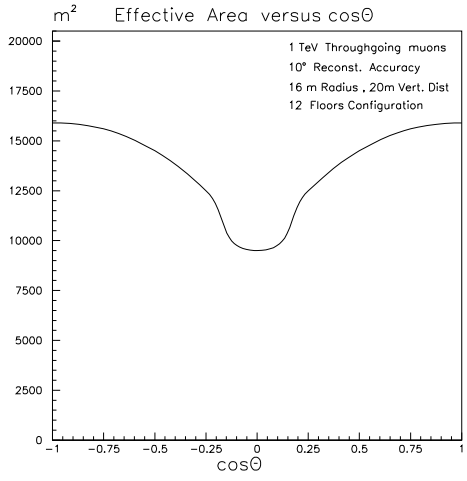

Figure 6: Effective area of 1 Tower for 1 Tev μ's and 10^o reconstruction accuracy vs the zenith angle ($cos\theta = 0$ is the horizontal, $cos\theta = 1$ means downgoing)

In order to study our efficiency for vertical throughgoing μ's we have generated μ's up to 100 m from the detector center. The efficiency for 5^o reconstruction accuracy and three different energies is shown in figure 8.

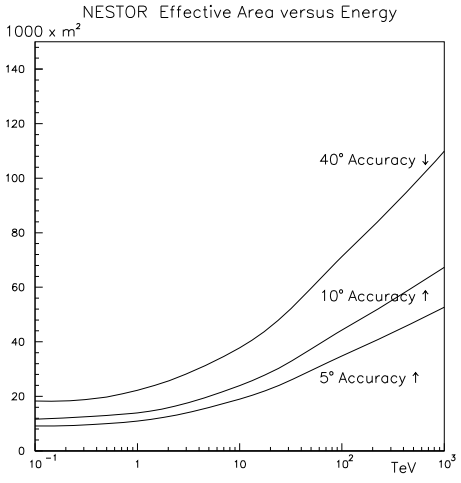

Figure 7: Effective area of one Tower averaged over all angles

11 Tests and construction status

The reliability is a key issue. Tests are being defined, Quality Assurance procedures have to be followed. The conception and construction of the detector is carried in collaboration with oceanographic and marine engineering institutions. Tests are being carried in marine installations near some of the participating laboratories. For various components of the detector, space or military specifications will have to be required. These considerations will not be detailed here [1].

11.1 The site

The deep underwater plateau is located at the S.W. of Peloponnesos, in the depths of the Ionian Sea. It is located 11 nautical miles from the small town of Methoni. The most important requirements for the detector are: clear water (i.e. water with small light attenuation coefficient), deep site (to filter out the atmospheric μ's), proximity to the shore (to use a short electro-optical cable to power the detector and transfer the data to the shore), low velocity of underwater currents (for minimal mechanical strain on the detector), flat and wide sea-bottom (to permit future expansion) and stable geological and other environmental characteristics (for long life time of the detector).

Four major cruises were made during the period 1989-1994. We obtained a good environmental description of the site, which is described in the following. Moreover, hydrographic survey and sub-bottom profiling of the site and of the proposed route of the deep underwater cable have been made.

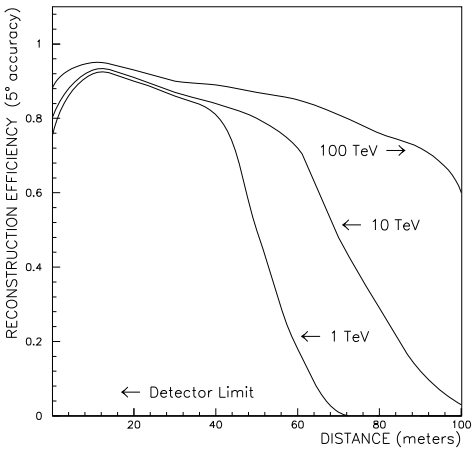

Figure 8: Efficiency for 5^o reconstruction accuracy and three different energies

11.2 Water Transmissivity

We have performed mainly three sets of sea water transmissivity measurements: a) Long base line with a monochromator (tight acceptance instrument), b) Tight geometry photometer *in situ* and c) Long base line *in situ*, (large acceptance instrument) [34, 35].

From the first set of measurements the attenuation coefficient was found equal to 0.025m^{-1} to 0.040m^{-1} (at the 470-490nm region) and almost constant for depths more than 1000m. From those values and the assumption that the ratio $\Lambda = \sigma/\epsilon$, where σ is the scattering coefficient and ϵ the attenuation coefficient, for very clean water is about 20% to 50% (oceanographers differ in this correction), it was calculated that the absorption length at 470nm wavelength and depths more than 2000m is **L = 42 to 67m**. The other measurements give consistent results and we conclude that the site has very clear waters suitable for our detector. New underwater measurements are in preparation.

11.3 Deep underwater current velocities and temperature

Several underwater current velocity measurements at the general area of NESTOR were made between 1989 and 1993 [1, 36] . Generally the measured underwater current velocities were less than 10cm/sec. Generally the site has deep underwater current with low velocities that will impose minimal mechanical stresses on the detector. The water temperature below the depth of 2500m, varies slightly with depth and is found to be 14.0° C.

11.4 Sea bottom morphology

In 1992 and 1994 studies of the sea-bottom were performed [1]. The area around site and the access to the shore was sounded with an echo-sounder and profilers and mapped using the GPS system. Moreover samples of the surface of the underwater basin were retrieved. The basin is covered by thick muddy and relatively stiff sediments having been deposited at low sedimentation rates (a few cm/kyears). Measurements of biofouling on the Benthos spheres are in preparation.

11.5 Background from ^{40}K

The fundamental optical background in the deep sea is due to ^{40}K decays. The ^{40}K is a primordial natural radio nuclide with a half-life of 1.27×10^9 years and its abundance is 0.0118% of K. The ^{40}K decays mainly to ^{40}Ca emitting electrons (branching ratio 89.5%) that produce Čerenkov light. The calculated background on our detector due to ^{40}K is roughly 13 disintegrations/lt/sec, which is a typical value for underwater light collecting experiments.

Underwater measurements are being carried.

11.6 Deep water cosmic ray measurements in the NESTOR site

In 1991 we deployed [1] a Russian built hexagonal structure (7m radius) made of titanium alloy, supporting 10 phototubes facing upwards, down to a depth of 4100m. We measured the vertical μ intensity and the angular distribution of downcoming μ's. As one can see from fig. 1 our results at 3300m, 3700m, and 4100m agree very well with DUMAND I [12], the deep mine measurements, and calculation in [2].

In November 1992 we deployed [1] a linear string of five 15 inch phototubes (again the photocathodes were facing upwards) from 3700m to 3900m. The vertical intensity of cosmic ray μ's flux and its variation as a function of the zenith angle were measured. The results are in good agreement with the previous measurements and calculations, and give, at depths between 3700m and 3900m a vertical flux of

$9.8 \pm 410^{-9} cm^{-2} s^{-1} sr^{-1}$.

The background due to radioactive ^{40}K and bioluminescence in the water is 600 ± 150 photons.cm^{-2}.s^{-1}. We note that this is an upper limit because, since the phototubes were suspended from the ship, the vertical motion is a source of excitations for various living organisms, giving very high values for the bioluminescence compared to anchored phototubes

11.7 Mechanical tests

During three oceanographic cruises from 89 to 92, three prototypes of possible detectors having different geometrical configurations have been tested. Two Aluminum prototypes constructed in Kiel are undergoing

deployment tests starting in 1995. Several new tests, of two floors at the beginning, in shallow water and in the deep sea, are foreseen. These tests, as well as the results of the first tower, will allow us to choose the final design for the construction of the following towers .

11.8 PMT and Optical Module tests

The 168 PMT's that have been baught have undergone extensive systematic tests [1]. Those that did not meet specifications were returned to the factory and repaired. Single photoelectron response and TTS (transit time spread) for all tubes are tested. The typical TTS measured value is 5.5ns. The PMT response as a function of the position of the incident light is nearly uniform inside the region of the photocathode ($|\theta| < 63°$). Typically, the measured dark counts are below 10 kHz, and always below the 40 kHz stated as a maximum in the manufacturer specifications. The measured prepulses are less than 2.0%, while late and after pulses are below 3%. Linearity studies show that for the chosen supply voltage the PMT signal displays a good linearity for pulses up to 100 photoelectrons. Response studies are continuing in order to define the optimum working point of the PMT.

Pressure tests of the optical module, connectors, cables are under way. Test deployments of optical modules and calibration spheres took place and others are in preparation.

The response of optical modules to Čerenkov light is being tested in a water-filled tank at a muon beam at CERN and with cosmic rays.

12 Long term projects

12.1 The km^3 detector

In order to study the physics items listed in section 1, and to obtain a better sensitivity on the physics subjects that we will have started studying with one tower, a bigger detector and/or a detector with a lower energy threshold is needed.

The definition of the detector parameters in order to study each physics subject may be done using the ν fluxes predicted by the theoretical models. In the absence of any model one can try to define a detector with a sensitivity significantly greater than already existing detectors. Financial and technological considerations would be severe constraints. In a first approach, one should push these constraints as far away as possible.

The best design of the next generation detector could be made by assembling several detectors, as they are actually projected, spaced by 100-200 m. This would be, for instance, a network of towers and strings, as described in chapter 1 of volume 1, reaching a surface of 1 km^2. With a detector of this size the search for the non-baryonic dark matter would be performed using not only the Earth core as a ν source but also the Sun. This would enlarge considerably the domain of the phase space of the parameters to be explored. The search of galactic sources would gain in sensitivity and it would be possible to detect the Active Galactic Nuclei as individual sources of ν's (see also [40, 41]).

Inside such a detector a second one with a volume of a few 10^5 m^3 and with an energy threshold of a few hundreds of MeV could allow us to reach a sensitivity an order of magnitude greater than that of SuperKamiokande. The total mass of such a detector will contain a few 10^{35} nucleons and, then, the sensitivity needed to detect the nucleon decay as predicted by the super-symmetrical models could be reached in a few years.

The detection of ν's from extra-galactic Supernovæ(as Andromeda for instance) needs a detector of at least 10^5 m^3 equiped with 10^4 optical modules.

In conclusion, the next generation detector should occupy a volume of 1 km^3 and should be equipped with at least 10^5 optical modules. Its structure must be multi-modular with a core with a higher density of optical modules and with external regions with lower density of light detectors. This will consitute a formidable challenge from a financial and technological point of view. For this reason it cannot be materialized without the collaboration of the institutes which are now participating to the realization of the various actual projects, which may be considered as prototypes of the future detector.

Since 1994 the project was initialized and discussed in several meetings (Venice, Saclay, Berkeley). The OECD Megascience Forum discussed such projects [42]. The members of BAND (for Baikal, AMANDA, NESTOR, DUMAND) have decided to create some working groups on various scientific and technical subjects. A technical and a scientific workshop take place in 1996.

12.2 Acoustic Detection studies

The acoustic detection of elementary particles was suggested in the '50s [43] . A possibility of deployment of the deep ocean acoustic detector to search for ultrahigh energy (UHE) ν's (with energies above 10 PeV) has been discussed almost 20 years ago [44] , The prediction of considerable UHE ν fluxes from AGN [45] supported much the idea of deployment of the large-scale cosmic ν detectors and in particular, the acoustic ν telescope [46] .

The deep underwater acoustic ν telescope SADCO (Sea Acoustic Detector of Cosmic Objects) with a threshold energy above 5 PeV was suggested to be deployed at the NESTOR site [47] .

The search for UHE ν's via detection of an acoustic bipolar pulse caused by the expansion of the water due to the highly localised heating caused by the energy deposit in electron-hadron cascades is the main goal of the SADCO project. The cascades are initiated by in-

teractions of ν's of all flavours with nucleons in matter and particulary by the resonance interactions of $\bar{\nu}_e$ with electrons The advantage is that, in the frequency of 10–20 kHz, the attenuation length is of the order of a few kilometers. The fiducial volume of the SADCO ν telescope should be the order of $10^8 - 10^9 m^3$ if tens of events per year caused by ν's with the resonance energy are to be measured. The sound pressure level and the duration of the bipolar pulse produced by the electron-hadron cascades as well as acoustic noise conditions at the SADCO site are important parameters.

The results of the preliminary measurements of the acoustic background at depth of 4 km at the NESTOR site and calculations of the characteristics of the acoustic pulses produced by the electron- hadron cascade with an energy of 10 PeV as well as future plans are presented in detail in [1].

Acknowledgements

I wish to thank the organizers of this conference and I am indebted to my colleagues of the NESTOR collaboration, whose contributions in [1] I used in writing this paper.

References

[1] The NESTOR Collaboration, Proposal, May 19, 1995.

[2] Proceedings of the 2nd and 3rd NESTOR International Workshops, Pylos, Greece, 19–21 October, 1992 and 19–21 October, 1993 edited by L. K. Resvanis (Physics Laboratory, University of Athens). The depth-intensity calculation and figure are from Bugaev et al., in the 3rd Workshop.

[3] *"The Second EGRET Catalog of High-Energy Gamma-Ray Sources"* D. J. Thompson et al., 1995, Ap. J. Suppl. 101, 259.

[4] A. D. Kerrick et al., *"Outburst of TeV Photons from Mrk 421"*, submitted to *Astrophysical Journal Letters* (1995)
M. Catanese et al., *"Detection of gamma rays with E 300 GeV from Mrk 501"*, Padua Workshop on TeV gamma ray astrophysics, September 1995, Harvard-Smithsonian Center Preprint 4203.

[5] F. Stecker et al., *Astrophys. J.* **390** (1992) L49.

[6] O. C. De Jager et al., *Letters to Nature* **369** (1994) 294.

[7] K. Greisen, Ann. Rev. Nucl. Sci. 10, (1960) 63.
M.A. Markov, I.M. Zheleznykh, Nucl. Phys. 27 (1961) 385.

[8] T. Gaisser, F. Halzen, T. Stanev, *Phys. Rep.* **258** (1995) 173.

[9] V. J. Stenger, in: *Proceedings of the 2nd NESTOR International Workshop*, Fortress of Niokastro, Pylos, Greece, 19–21 October, 1992, edited by L. K. Resvanis (Physics Laboratory, University of Athens, Athens, 1993), p. 79.

[10] A. Roberts, *Rev. Mod. Phys.* **64** (1992) 259.

[11] T. Stanev, Proc. of the 4$^{\text{th}}$ Int. Workshop on Neutrino Telescopes, Venice, March 1992, ed. M. Baldo-Ceolin.

[12] P. Bosetti et al., DUMAND II : proposal to construct a deep ocean laboratory for the study of high energy neutrino astrophysics and particle physics, University of Hawaii Publication, HDC-2-88, p. 1-155 (1988)
C. H. Wiebusch et al., DUMAND II : supplementary proposal, University of Hawaii, August 1994
A. Roberts, Rev. Mod. Phys. 64 (1992) 259
P. K. F. Grieder, DUMAND II status report, Preprint BU-DUMAND-94/1, February 1994.

[13] R. Wischnewski (BAIKAL Coll.), Proc. of the 5$^{\text{th}}$ Int. Workshop on Neutrino Telescopes, Venice, Mars 1993, p. 299

[14] D. M. Lowder et al., Nature 353 (1991) 331
S. W. Barwick et al., "AMANDA : Antarctic Muon and Neutrino Detector Array", Proc. of the 23rd ICRC, Calgary, 1993.

[15] L. K. Resvanis (NESTOR Coll.), in: *Proc. of the 5th Int. Workshop on Neutrino Telescopes*, Venice, Italy, 2–4 March, 1993, ed. M. Baldo Ceolin.

[16] K. S. Hirata et al. (Kamiokande Coll.), *Phys. Lett.* **B 205** (1988) 416; *ibid* **B 280** (1992) 146;
Y. Fukuda et al., *Phys. Lett.* **B 335** (1994) 237.

[17] D. Casper et al. (IMB Coll.), *Phys. Rev. Lett.* **66** (1991) 2561;
R. Becker-Szendy et al. (IMB Coll.), in: *Proc. of the 16th Int. Conference on Neutrino Physics and Astrophysics "Neutrino'94"*, Eilat, Israel, 29 May – 3 June, 1994, [*Nucl. Phys. B (Proc. Suppl.)* **38** (1995) 331].

[18] M. C. Goodman (for the SOUDAN 2 Coll.), in: *Proc. of the 16th Int. Conference on Neutrino Physics and Astrophysics "Neutrino'94"*, Eilat, Israel, 29 May–3 June, 1994 [*Nucl. Phys. B (Proc. Suppl.)* **38** (1995) 337].

[19] Ch. Berger et al. (Fréjus Coll.), *Phys. Lett.* **B 227** (1989) 489;
ibid **B 245** (1990) 305.
K. Daum et al., *Z. Phys.* **C 66** (1995) 417.

[20] M. Aglietta et al. (NUSEX Coll.), *Europhys. Lett.* **8** (1989) 611.

[21] A. V. Butkevich, L. G. Dedenko, and I. M. Zheleznykh, *Yad. Fiz.* **50** (1989) 142 [*Sov. J. Nucl. Phys.* 50 (1989)90].

[22] See, for example, E. D. Carlson, *Phys. Rev.* **D 34** (1986) 1454.

[23] F. A. Aharonian, *"VHE gamma-rays as tracers of nonthermal galactic and extragalactic sources"*, Padua Workshop Towards a Cherenkov Detector for TeV astro/particle physics, September 1995, MPI H V3 - 1996.

[24] V. S. Berezinskiĭ, et al., *"Astrophysics of Cosmic Rays"*, edited by V. L. Ginzburg (North-Holland, 1990).

[25] M. Sikora and M. C. Begelman, in: *Proceedings of the Workshop on High Energy Neutrino Astrophysics*, Honolulu, Hawaii, 23–26 March, 1992, p. 114.
F. W. Stecker, C. Done, M. H. Salamon, and P. Sommers, in: *Proceedings of the Workshop on High Energy Neutrino Astrophysics*, p. 1.
A. P. Szabo and R. J. Protheroe, *Astroparticle Phys.* **2** (1994) 374.
P. L. Biermann, in: *Proceedings of the Workshop on High Energy Neutrino Astrophysics*, Honolulu, Hawaii, 23–26 March, 1992, p. 86.

[26] General reviews of dark matter are given in V. Trimble, *Ann. Rev. Astron. Astrophys.* **25** (1987) 425;
J. R. Primack, D. Seckel, and B. Sadoulet, *Ann. Rev. Nucl. Part. Sci.* **38** (1988) 751.

[27] G. F. Giudice and E. Roulet, *Nucl. Phys.* **B 316** (1989) 429;
G. B. Gelmini, P. Gondolo, and E. Roulet, *ibid* **B 351** (1991) 623;
A. Bottino, et al., *Phys. Lett.* **B 265** (1991) 57;
F. Halzen, M. Kamionkowski, and T. Steltzer, *Phys. Rev.* **D 45** (1992) 4439;
M. Drees et al., *Phys. Rev.* **D 49** (1994) 636;
R. Gandhi et al., *ibid* **D 49** (1994) 3691.
K. Kamionkowski, *Phys. Rev.* **D 44** (1991) 3021.
M. Mori et al., *Phys. Rev.* **D 48** (1993) 5505.

[28] A. Bottino, N. Fornengo, G. Mignola, and L. Moscoso, *Astroparticle Phys.* **3** (1995) 65.

[29] S. J. Parke, FERMILAB Conf-91/251-T (September 1991);
M. C. Goodman, summary talk given at the *Workshop on Long Baseline Neutrino Oscillations*, Fermilab, 17–20 November, 1991, ANL-HEP CP-92-17;
R. Bernstein, *"Ideas for a Long-Baseline Neutrino Detector"*, February 1992, FERMILAB-Conf-92/63.

[30] J. Brunner (CHORUS Coll.), in:*Proceedings of the International Europhysical Conference on High Energy Physics*, Marseille, France, 1993, edited by J. Carr and M. Perrottet (Editions Frontières, Gif-Sur-Yvette, France, 1993), p. 555.

[31] L. DiLella (NOMAD Coll.), in: *Proceedings of the 15th International Conference on Neutrino Physics and Astrophysics "Neutrino'92"*, Granada, Spain, 7–12 June, 1992, edited by A. Morales [*Nucl. Phys. B (Proc. Suppl.)* **31** (1993) 319)].

[32] L. Wolfenstein, *Phys. Rev.* **D 17** (1978) 2369; **D 20** (1979) 2634;
S. P. Mikheyev and A. Yu. Smirnov, *Yad. Fiz.* **42** (1985) 1441 [*Sov. J. Nucl. Phys.* **42**(1985) 913]; *Nuovo Cimento* **9 C** (1986) 17.

[33] A. Ball, S. Katsanevas, and N. Vassilopoulos, CERN/ECP 95-13, to be submitted to NIM A.

[34] Bradner and G. Blackinton, Long base line measurements of light transmission in clear water, Applied Optics, vol 23, no7 (1984) 1009

[35] E.G. Anassontzis, et al, Light transmissivity in the NESTOR site, NIM A349 (1994) 242.

[36] Demidova T.A. and Kontar E.A. On near-bottom currents in the Mediterranean Sea. Gen.ass.EGU., Vienna 1991

[37] RD23 Coll., CERN/DRDC 93-95

[38] P. Bertin, D. Roncin, J. Vuillemin, *Programmable Active Memories: a Performance Assessment*, PRL Research Report 24, Digital Equipment Corp., Paris Research Laboratory, 85 Av. Victor Hugo. 92563 Rueil-Malmaison Cedex, France, 1993.

[39] Xilinx Inc., *The Programmable Logic Data Book*, Xilinx Inc., 2100 Logic Drive, San Jose, CA 95124 1993.

[40] F. Halzen et J. G. Learned, Proc. of the 5th Int. Workshop on Neutrino Telescopes, Venice, Mars 1993, p. 483

[41] J. G. Learned et A. Roberts, Proc. of the 23rd Int. Cosmic Ray Conf., Calgary, 1993.

[42] M. Spiro et L. Sulak, OECD Report, April 1994 and Paris session, 1996.

[43] Askaryan G.A., Atomnaya energiya 1957, N3, p.152, in Russian.

[44] Askaryan G.A., Dolgoshein B.A. Report on the 1976 DUMAND Summer Workshop Hawaii, September 1976; Preprint P.N.Lebedev Physical Institute (in Russian) N 160: Pisma v JETF, 1977, v.25, N 5, p.232 (in Russian)
Bowen T. Conference Papers (15th Intern. Cosmic Ray Conf., Plovdiv) 1977, V.6, p.277
Askarian et al, Acoustic Detection of High Energy Particle Showers in Water, NIM, 1979, V.164, N 2, p.267
Learned J. Phys.Rev. 1979,V.D19,p.3293.

[45] Stecker F.W.et al.Proc.3d Int. Workshop on Neutrino Telescopes, Venezia,1991,p.487.

[46] Learned J., Stanev T. Proc. 3d Int. Workshop on Neutrino Telescopes , Venezia, 1991,p.473.

[47] Butkevich A. et al. Proc. 2nd Int. Conf. on Trends in Astroparticle Physics (1991), Aachen, Germany. Tubner-Texte Zur Physik,1994,V.B28,p.128.